RESEARCH ARTICLE

Numerical Analysis of Slipping of the Wheel Under Rotation-controlled and Translation-controlled Motion on Railway Tracks

Pranjal Mandhaniya[1,*], Mugdad Alkhateeb[2], Narala Gangadhara Reddy[3], Abdullah Ansari[4], Mohmmad Farooq Bhat[5], Bilal Ahmad Malik[6] and Anish Kumar Soni[7]

[1] Norwegian University of Science and Technology, Trondheim, Norway
[2] University of East London, London, United Kingdom
[3] Fiji National University, Suva, Fiji
[4] Earthquake Monitoring Center, Sultan Qaboos University, Muscat, Oman
[5] Indian Institute of Technology (ISM), Dhanbad, India
[6] Tsinghua Shenzhen International Graduate School, Tsinghua University, China
[7] Indian Institute of Technology, Delhi, India

Abstract

There has been recorded differences between a train spulled by a locomotive and a train unit with all the bogies moving simultaneously. This study aims at the slip of wheel on a railway track under these different movements using finite element simulation on a ballasted railway track. The railway track was subjected to a loaded wheel moving at different speeds using two modes: translation-controlled (wagons pulled by locomotive) and rotation-controlled (simultaneously moving bogies) motion. The results were obtained in the form of track vibrations and wheel slip under moving loads at changing speeds and wheel-rail friction. It was concluded that the force transferred to the substructure does not change much based on the tribology of the wheel. However, the reduced wheel-rail friction will cause significant slippage and less efficient traction.

Keywords: railway tracks, finite element simulation, rolling, sliding, tribology, wheel slipping.

1 Introduction

The motion of trains starts with the rolling of wheels on the rails. The locomotive applies the torque to the wheels, which pulls the connected coaches. However, converting the torque into the translation of the train is not always efficient. The factors affecting this conversion include, but are not limited to, μ (friction between wheel and rail) and corrugation of rail and wheel flats [1]. There have been studies ranging from the effect of the wheel load and diameter on wheel-rail contact area by [2] to the finite element simulations

Submitted: 28 March 2025
Accepted: 26 July 2025
Published: 15 September 2025

Vol. 1, **No.** 2, 2025.
10.62762/SII.2025.935609

***Corresponding author:**
✉ Pranjal Mandhaniya
pranjalmandhaniya@gmail.com; pranjal.mandhaniya@ntnu.no

Citation
Mandhaniya, P., Alkhateeb, M., Reddy, N. G., Ansari, A., Bhat, M. F., Malik, B. A., & Soni, A. K. (2025). Numerical Analysis of Slipping of the Wheel Under Rotation-controlled and Translation-controlled Motion on Railway Tracks. *Sustainable Intelligent Infrastructure*, 1(2), 67–73.

studies about traction and wheel-rail friction (μ) by [3]. Studies have examined structural fatigue and its effect on rolling wheels [4]. However, there is a gap in the literature's study of simulation-based translation and rotational motion. The present study tries to fill this gap.

A properly rounded wheel performs two types of motion on the rail as outlined in Figure 1. Rotation-controlled motion, primitive in the locomotive of a train, occurs when the wheel is restricted to move at a given rotation value around its axis while allowing forward displacement freely [5]. Translation-controlled motion, primitive in trailing cars, occurs when the wheel is restricted to moving at a given value of forward displacement while allowing free rotation around its axis. Dynamic forces and repeated loading conditions play a significant role in influencing the contact mechanics and motion stability, necessitating detailed analysis of rotational and translational effects on structural integrity [6].

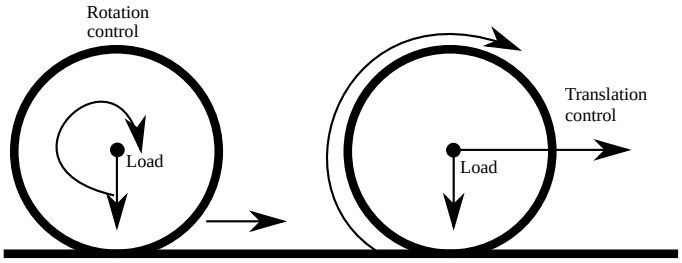

Figure 1. Rotation-controlled and translation-controlled motion of a wheel.

The present study compared these two wheel motion mechanisms and how their application affects the track response. The tribology study was carefully conducted by gradually increasing the speed of motion with changing rotation amplitude with time. A gradual increase in speed was used to reduce the sliding of the wheel in rotation-controlled motion.

2 Details of the simulation model

The present model is part of a chain of research done previously [7–12]. The rail track geometry was adopted from this research as shown in Figure 2. Only half of the cross-section was simulated using symmetry about the center of the gauge, as shown in Figure 2(a). The sleeper arrangement is shown in Figure 2(b). A simplified version of the 60E1 rail section was modeled, as shown in Figure 2(c).

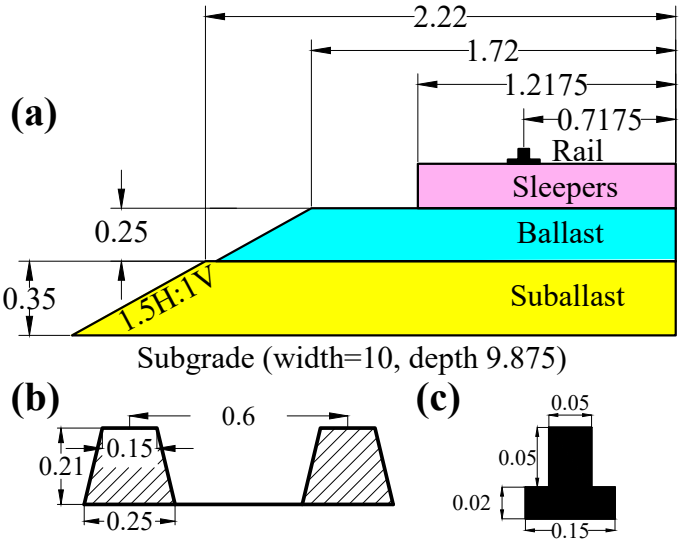

Figure 2. Detailed diagram of the rail track model (all dimensions are in meters) (a) complete cross-section of rail track (b) cross-section and arrangement of sleepers (c) cross-section of rail.

The material properties (density as ρ, Young's modulus as E, Poisson's ratio as ν and angle of internal friction as ϕ) of track parts are shown in Table 1, same as those adopted in previous research [7–10].

The elastoplastic or even the elastic properties are not a concern for the aim of the present study, i.e., the comparison of translation and rotation-controlled wheel motion. However, this study is a part of comprehensive research published in [7–10]. Thus, the same properties, including mesh convergence study, were adopted.

Table 1. Material properties and global mesh sizes of track components.

Part	ρ (kg/m^3)	E (GPa)	ν	ϕ (°)	GM (mm)
Wheel	7850	200	0.3	-	50
Rail	7850	200	0.3	-	100
Sleepers	2400	30	0.2	-	500
Ballast	2400	0.14	0.37	51	500
Subballast	2400	0.07	0.37	40.5	500
Subgrade	2000	0.03	0.4	35	1000

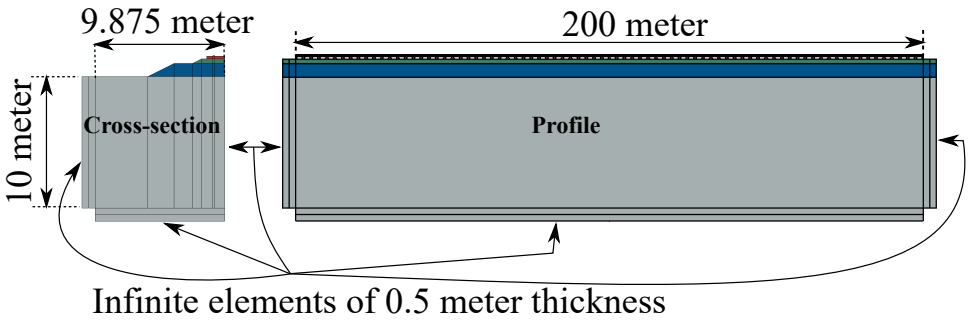

Figure 3. Extents of finite element model in ABAQUS.

The cross-section shown in Figure 2 was modeled as a 200-meter long 3D finite element model in ABAQUS, as shown in Figure 3, similar to what has been done in [7]. A three-dimensional solid eight-node element with reduced integration (C3D8R in ABAQUS) was used for the entire model. In contrast, infinite element (CIN3D8 in ABAQUS) layers, as shown in Figure 3, were used at the boundaries. The roller boundary condition was applied to all vertical boundaries, allowing displacement only in the vertical direction and restraining movements in other directions. A fixed boundary was applied at the bottom surface of the subgrade, ensuring zero rotation and displacement. All the interfaces (rail-sleeper, sleeper-ballast, ballast-subballast, and subballast-subgrade) were bound with zero relative slip and separation.

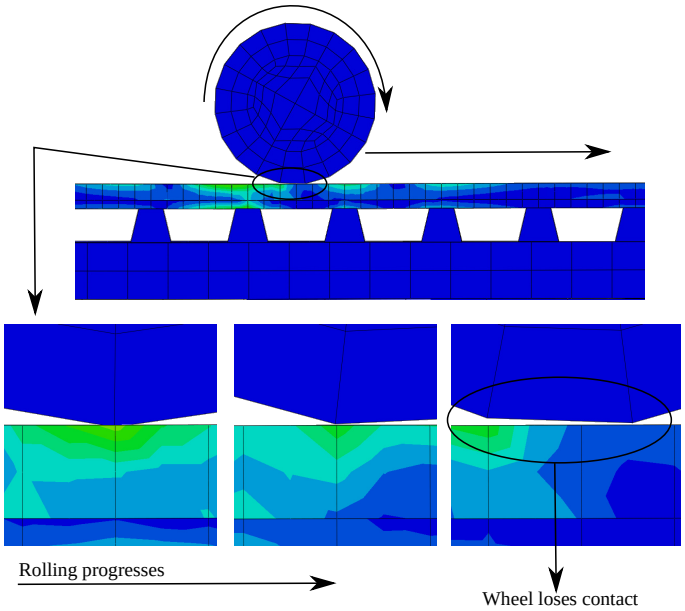

Figure 4. Wheel-rail contact with large arc length.

3 Wheel-rail meshing for continuous rolling contact

Based on literature [13] and several trial simulations, it was found that the meshing of wheel and rail should be done in a manner such that the element arc length of the wheel is roughly equal to the longitudinal element length of the rail. This arc length should be small enough to support constant contact throughout the rolling motion of the wheel, thus generating an efficient force transfer [14]. The global mesh size of the rail and wheel is 50 mm to minimize the sliding while keeping the same mesh for all other parts. A coarse mesh for rail and wheel causes a temporary detachment, as shown in Figure 4, subsequently affecting the load transfer from the wheel to the substructure.

This problem can be avoided in translation-controlled motion by allowing pure sliding. Pure sliding is also possible in rotation-controlled motion at zero μ [15] exists. A moving object with flat contact can also be used instead of a wheel to resolve the problem of constant contact. The moving object's contact area should be derived from the wheel-rail contact [2]. In the present study, the comparison between rotation-controlled and translation-controlled motion was performed using only one wheel to keep the analysis as unbiased as possible.

The load motion can be simulated by either a moving wheel or a specialized subroutine (DLOAD or VDLOAD) compiled in ABAQUS [16]. The inertial forces related to wheel motion simulation were absent in the subroutine-based motion simulation, reducing the simulation time. In the present study, the wheel speed was controlled by fixing the translation or rotation value with respect to time. The wheel of diameter 1 m was loaded at the center with 162.5 kN [7] concentrated force before the commencement of motion. The load was then moved. A hard contact in ABAQUS [16] was used for normal direction. The present study tries to look into three parameters concerning the tribology of the wheel.

1. Wheel-rail friction (μ) - The value of μ were changed. Three values were adopted, i.e., 0.1, 0.2

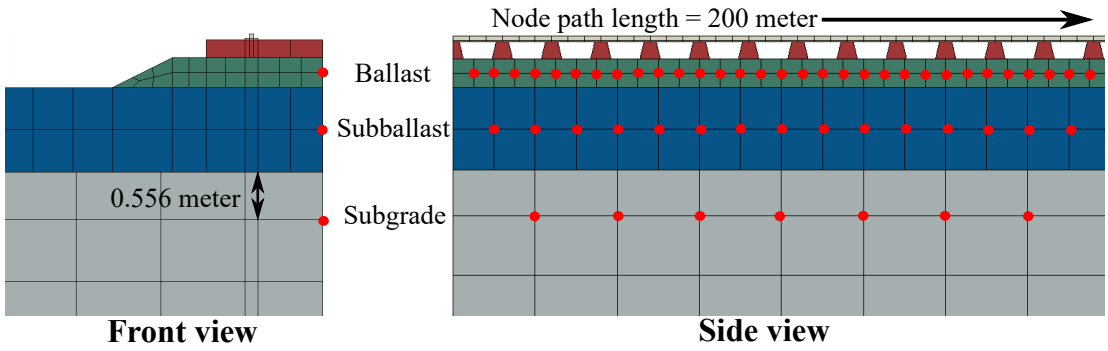

Figure 5. The location of node paths.

and 0.3.

2. The wheel's speed and acceleration - The wheel's initial speed was kept at 50 kmph. In the first case, the speeds of the wheel were increased at an interval of 50 kmph to a final speed of 250 kmph (this data is referred to as D1 in the results section). In the second case, the speeds of the wheel were increased at an interval of 25 kmph to a final speed of 150 kmph (this data is referred to as D2 in the results section). The speed increments were enacted after the wheel had run for 18 meters at a constant speed.
3. Mesh size of rail and wheel. The initial mesh size of the rail and wheel, i.e., 100 and 50 mm (same as D1 in the results section), were changed to 50 and 25 mm (this data is referred to as D3 in the results section), respectively. Simply put, the mesh sizes of the wheel and rail were halved.

Apart from all the parameter changes, the translation-controlled motion or sliding motion simulation rendered the reference data called D4 in the results section.

4 Results

The vertical velocity and acceleration (cumulatively called track responses) were calculated at the node path after the wheel's motion was finished. The node paths are shown in Figure 5. This generates output over the length of the path, which is thus called the node-path output. The selection of track responses is based on previously published research by the same authors [7, 8, 17]. The selected track responses best represent the dynamic effect of moving load.

Thereafter, the area under the curve (AUC) and peak-to-peak (PTP) values are extracted from the node-path output as shown in Figure 6. The unit of AUC was calculated by multiplying the SI unit of track response by the distance along the path (m). The PTP is calculated as the maximum and minimum track response difference. The units of PTP were the same as the SI units of track response. The AUC represented the track response over the volume, while the PTP represented the track response at the loading point.

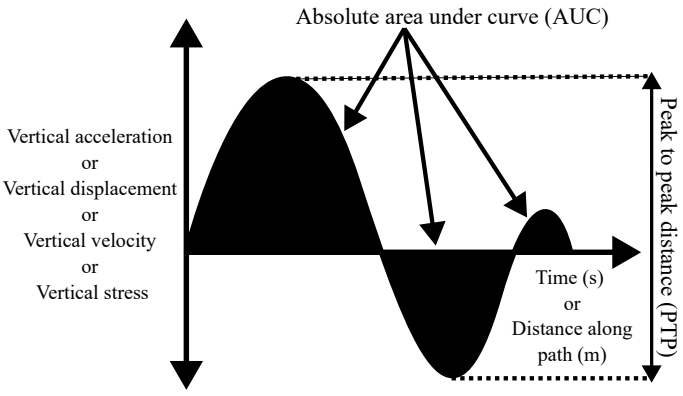

Figure 6. The extraction of AUC and PTP from node-path outputs.

The plots of vertical velocity node-path output at substructure nodes were plotted with gradually increasing speeds for translation-controlled and rotation-controlled motions are shown in Figure 7. The rotation-controlled motion was performed with three values of wheel-rail friction.

The track response peaks of rotation-controlled motion generally lag from the actual location of the wheel because there is some rolling loss. A parameter that represents this difference in lag, sliding potential (S_p), is formulated using the assigned displacement (d_a) and the observed displacement (d_o) as given in Eq. 1. Table 3 outlines the values of sliding potential.

$$S_p = \frac{(d_a - d_o) \times 100}{d_a} \tag{1}$$

The results of the parametric study are consolidated in Figure 8, Table 2. The value of S_p decreased with increasing friction, which is self-explanatory. The

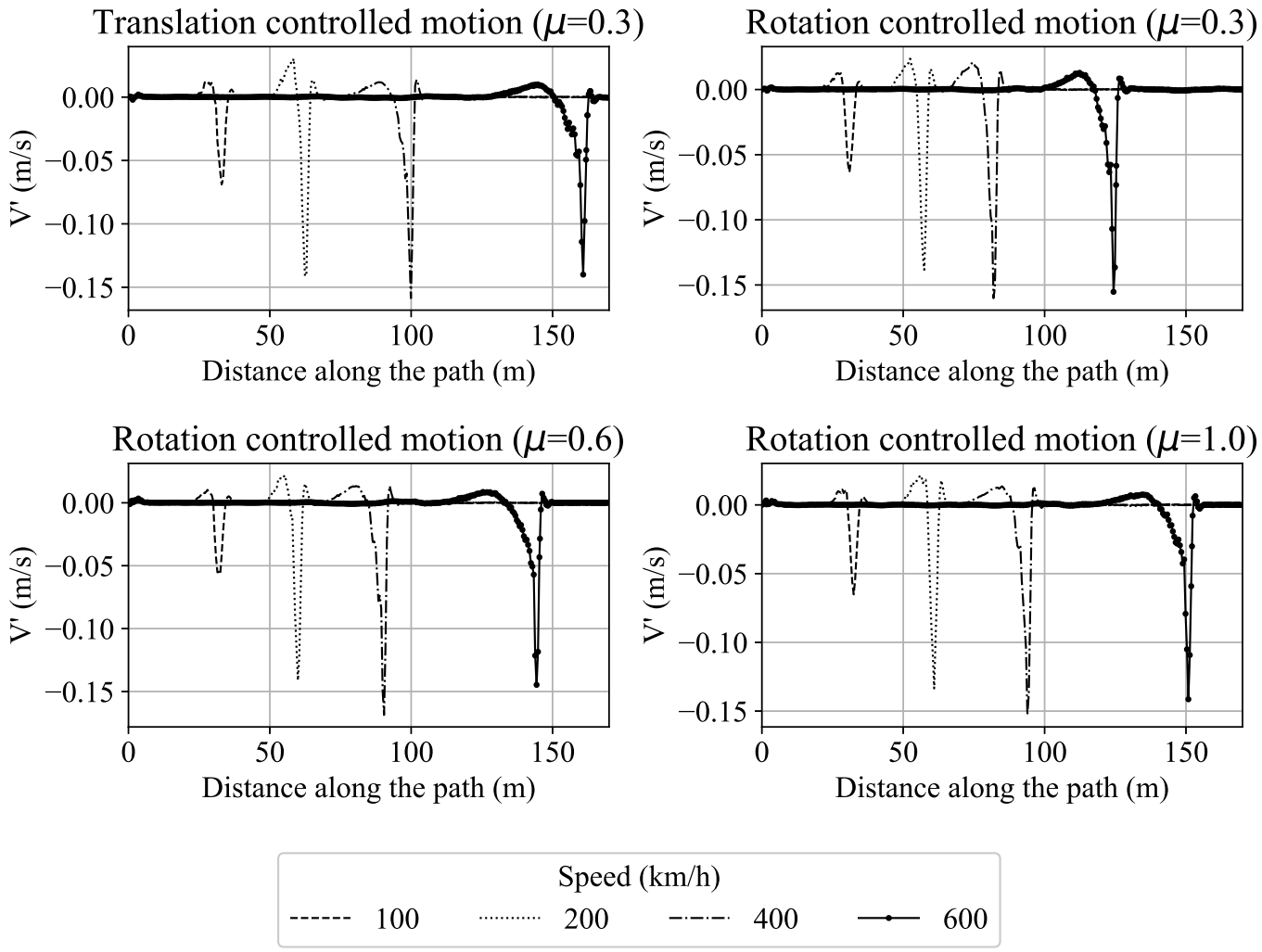

Figure 7. Vertical velocity at nodes for rotation and translation controlled motion in substructure layers with changing friction.

increased friction caused the wheel to reduce rolling losses. The datasets D1 and D2 show the difference in tribology with the variation in the speed of motion of the wheel. The average vertical velocity values shown in Table 2 for both mean AUC and PTP are higher for D1 than D2 because of the higher motion speed range [8].

Table 2. AUC, PTP and S_p averaged over vertical velocity node path output.

	D1	D2	D3	D4
AUC	0.514	0.358	0.508	0.496
PTP	0.175	0.136	0.184	0.164
S_p	6.788	2.467	6.727	0.554

The effect of the rail and wheel mesh sizes was compared using D1 and D3 datasets. The mean AUC and PTP values from vertical velocity in D1 and D3 were very close and did not follow any pattern. For comparing the sliding and rolling action on the same speed range, the D1 and D4 datasets were compared. The mean AUC and PTP values in Table 2 are slightly lower for D4 than D1. This shows a slightly higher impact due to the rolling inertia of the wheel.

The major aspect of the present study is to shed light on the tribology difference based on the rolling and sliding motion of the wheel, which is highlighted by slippage. Table 2 shows the reduction in slippage with a slower velocity range by comparing S_p values for D1 and D2. The slippage change is negligible based on mesh sizes as S_p values for D1 and D3 are very close. However, Table 3 examines slippage with friction at higher speeds. The slippage at higher speeds is much higher and shows greater rolling loss. Increased rolling friction caused some coverage in the slippage. However, higher friction means more traction will be required to pull the wheel to roll, thus causing increased energy consumption.

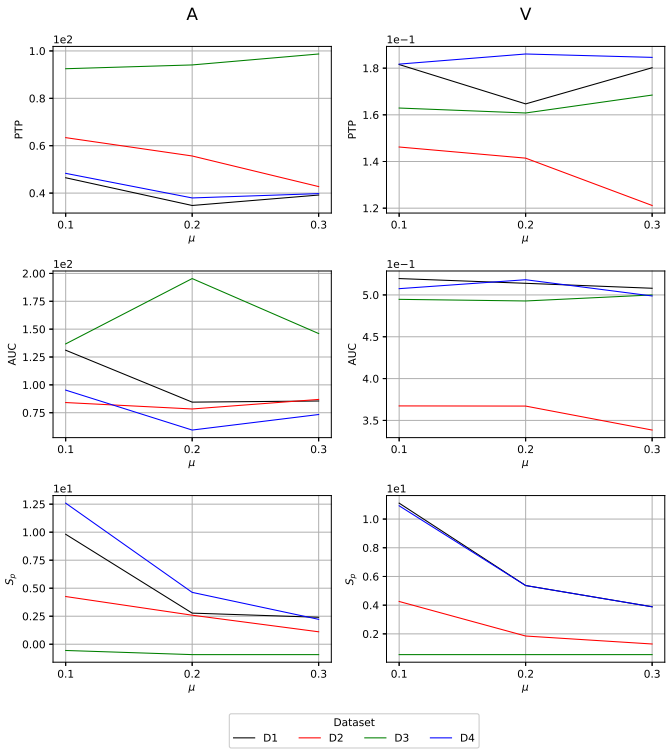

Figure 8. The consolidated results of the parametric study.

Table 3. S_p - μ matrix.

Speed (km/h)	$\mu = 0.3$	$\mu = 0.6$	$\mu = 1.0$
100	5.13	2.56	2.56
200	10.17	6.78	3.39
400	34.67	18.67	12

5 Conclusions

The gap between the vertical velocity of translation-controlled and rotation-controlled motion diminishes with increasing wheel-rail friction. Thus, it can be said that the lag between peaks is due to slippage, which occurs when the wheel rolls in its place without undergoing any translation due to inertial resistance. There is little difference between the magnitude of vertical velocity between translation-controlled and rotation-controlled motion. Thus, translation-controlled motion is adequate to manifest the effect of a moving wheel.

Data Availability Statement

Data will be made available on request.

Funding

This work was supported without any funding.

Conflicts of Interest

The authors declare no conflicts of interest.

Ethical Approval and Consent to Participate

Not applicable.

References

[1] Kalker, J. J. (1990). *Three-Dimensional Elastic Bodies in Rolling Contact*. Springer Dordrecht. [CrossRef]

[2] Andrews, H. I. (1959). The contact between a locomotive driving wheel and the rail. *Wear, 2*(6), 468–484. [CrossRef]

[3] Deng, X., Ni, Y.-Q., & Liu, X. (2022). Numerical Analysis of Transient Wheel-Rail Rolling/Slipping Contact Behaviors. *Journal of Tribology, 144*(10), 101503. [CrossRef]

[4] Makino, T., Kato, T., & Hirakawa, K. (2012). The effect of slip ratio on the rolling contact fatigue property of railway wheel steel. *International Journal of Fatigue, 36*(1), 68–79. [CrossRef]

[5] Zhang, Z. (2015). *Finite element analysis of railway track under vehicle dynamic impact and longitudinal loads* (Doctoral dissertation, University of Illinois at Urbana-Champaign).

[6] Bhat, M. F., & Koner, R. (2023, November). Enhancing Load-Bearing Capacity of a Haul Road in Opencast Mine using Non-Woven Geotextiles: A CBR Analysis. In *International Conference on Sustainable and Innovative Mining Practices* (pp. 537-546). Cham: Springer Nature Switzerland. [CrossRef]

[7] Mandhaniya, P., Shahu, J. T., & Chandra, S. (2023). Analysis of dynamic response of ballasted rail track under a moving load to determine the critical speed of motion. *Journal of Vibration Engineering & Technologies, 11*(7), 3197-3213. [CrossRef]

[8] Mandhaniya, P., Shahu, J. T., & Chandra, S. (2022). An assessment of dynamic impact factors for ballasted track using finite element method and multivariate regression. *Journal of Vibration Engineering & Technologies, 10*(7), 2609-2623. [CrossRef]

[9] Mandhaniya, P., Shahu, J. T., & Chandra, S. (2022). Numerical analysis on combinations of geosynthetically reinforced earth foundations for high-speed rail transportation. *Structures, 43*, 738–751. [CrossRef]

[10] Thölken, D., Abdalla Filho, J. E., Pombo, J., Sainz-Aja, J., Carrascal, I., Polanco, J., ... & Woodward, P. (2021). Three-dimensional modelling of slab-track systems based on dynamic experimental tests. *Transportation Geotechnics, 31*, 100663. [CrossRef]

[11] Yang, X., Gu, S., Zhou, S., Yang, J., Zhou, Y., & Lian, S. (2015). Effect of track irregularity on the dynamic response of a slab track under a high-speed train based on the composite track element method. *Applied Acoustics, 99*, 72-84. [CrossRef]

[12] Jiang, B., Ma, M., Li, M., Liu, W., & Li, T. (2019). Experimental study of the vibration characteristics of the floating slab track in metro turnout zones.

Proceedings of the Institution of Mechanical Engineers, Part F: Journal of Rail and Rapid Transit, 233(10), 1081-1096. [CrossRef]

[13] Kalker, J. J. (1991). Wheel-rail rolling contact theory. *Wear, 144*(1), 243–261. [CrossRef]

[14] Shabana, A. A., Zaazaa, K. E., Escalona, J. L., & Sany, J. R. (2004). Development of elastic force model for wheel/rail contact problems. *Journal of Sound and Vibration, 269*(1–2), 295–325. [CrossRef]

[15] Wu, J., Liang, J., & Adhikari, S. (2014). Dynamic response of concrete pavement structure with asphalt isolating layer under moving loads. *Journal of Traffic and Transportation Engineering (English Edition), 1*(6), 439–447. [CrossRef]

[16] SIMULIA. (2009). *Abaqus User Manual* (Ver 6.9).

[17] Esen, A. F., Woodward, P. K., Laghrouche, O., Čebašek, T. M., Brennan, A. J., Robinson, S., & Connolly, D. P. (2021). Full-scale laboratory testing of a geosynthetically reinforced soil railway structure. *Transportation Geotechnics, 28*, 100526. [CrossRef]

Pranjal Mandhaniya received the combined bachelors and masters degree in civil engineering from Indian Institute of Technology, Kanpur, India, in 2016. He received his PhD in civil engineering from Indian Institute of Technology, Delhi, India, in 2023. Currently, he is working in Norwegian University of Science and Technology as postdoctoral fellow. (Email: pranjal.mandhaniya@ntnu.no)

Mugdad Alkhateeb earned his degree in Surveying and Mapping Sciences from the University of East London in 2011. He then pursued a Master's in Structural Engineering at London South Bank University, completing it in 2015, followed by a Master's in Philosophy from the same institution in 2020. After gaining industry experience, Mugdad transitioned to academia as a senior lecturer at the University of East London. He is currently serving as a Consultant Engineer at an undisclosed organization. (Email:M.Alkhateeb@uel.ac.uk)

Narala Gangadhara Reddy received his Ph.D. in geotechnical engineering from the Indian Institute of Technology (IIT) Bhubaneswar, India, in March 2020. He obtained his M.Tech. in Geotechnical Engineering from National Institute of Technology, Bhopal, India, in 2014. He has international research experience, having served as a Postdoctoral Research Associate at Shantou University, China (September 2019 – August 2020), and as a Visiting Research Fellow at Nanjing University, China (December 2019 – February 2020). He received Indo (MHRD) - Chinese Government Scholarship (CSC) to visit China in 2019. Currently, he is an Assistant Professor in the Department of Civil Engineering at Fiji National University, Republic of Fiji. His expertise spans geotechnical engineering, sustainable infrastructure, and climate-resilient solutions. (Email: narala.reddy@fnu.ac.fj)

Abdullah Ansari received his Ph.D. from the Civil Engineering Department of the Indian Institute of Technology Delhi (IIT Delhi) India in March 2023. He obtained his M. Tech. and B.E. degree, specializing in Geological Technology from the Earth Science Department of the Indian Institute of Technology Kanpur (IIT Kanpur) India in 2018, and in Civil Engineering from the Government College of Engineering and Research Pune (GCOEARA Pune) India in 2016, respectively. He began his professional journey as a Postdoctoral Researcher at Inha University and Inje University in South Korea. Currently, he's working as an Assistant Professor (Research) at the Earthquake Monitoring Center (EMC), Sultan Qaboos University (SQU) Muscat, Oman. (Email: a.ansari@squ.edu.om)

Mohmmad Farooq Bhat is working as Junior Research Fellow at Indian Institute of Technology (Indian School of Mines) Dhanbad. He received his Bachelors and Masters in Civil Engineering in 2019 and 2022 respectively. (Email: farooqbhat45@gmail.com)

Bilal Ahmad Malik received his Ph.D. in geotechnical engineering from the National Institute of Technology (NIT) Srinagar, India, in October 2022. He obtained his B.Tech. in Civil Engineering from the Islamic University of Science & Technology, Awantipora, India, in 2015. He is a postdoctoral research fellow at the Institute of Ocean Engineering, Shenzhen International Graduate School, Tsinghua University, China. His research focuses on offshore foundation systems, particularly suction caissons and pile foundations, with an emphasis on experimental and numerical investigations. Previously, he worked as a postdoctoral research fellow at the Indian Institute of Technology (Indian School of Mines), Dhanbad. (Email: bilal.malik1588@gmail.com, bilalmalik1731@sz.tsinghua.edu.cn)

Anish Kumar Soni received the bachelor's degree in civil engineering from National Institute of Technology, Hamirpur, India, in 2020. He received his M.Tech in Geotechnical & geoenvironmental engineering from Indian Institute of Technology, Delhi, India, in 2023. Currently, he is a Phd graduate at University of Melbourne. (Email: sonianish5800@gmail.com)